Structure evolution and Properties of TiAlCN/VCN Coatings Deposited by Reactive HIPIMS

HOVSEPIAN, Papken <http://orcid.org/0000-0002-1047-0407>, EHIASARIAN, Arutiun <http://orcid.org/0000-0001-6080-3946> and PETROV, Ivan

Published version

HOVSEPIAN, Papken, EHIASARIAN, Arutiun and PETROV, Ivan (2014). Structure evolution and Properties of TiAlCN/VCN Coatings Deposited by Reactive HIPIMS. Surface and Coatings Technology, 257, 38-47.

Structure evolution and Properties of TiAlCN/VCN Coatings Deposited by Reactive HIPIMS

P. Eh. Hovsepian[1], A. P. Ehiasarian[1], I. Petrov[2]

[1)] Sheffield Hallam University, Howard Street, Sheffield, S1 1WB, UK

[2)] University of Illinois at Urbana-Champaign, 104 South Goodwin Avenue, Urbana, Illinois 61801

Abstract:

2.5 µm thick TiAlCN/VCN coatings were deposited by a reactive High Power Impulse Magnetron Sputtering (HIPIMS) process. Cross-sectional TEM showed gradual evolution of the structure of the coating with thickness. The initial structure is a nanoscale multilayer with sharp interlayer interfaces. This transforms to nanocomposite of TiAlCN and VCN nanocrystalline grains surrounded by a C-rich tissue phase and finally changes to an amorphous carbon rich Me-C phase. In contrast deposition in similar conditions using standard magnetron sputtering produces a well-defined nanoscale multilayer structure. Depth profiling by AES showed that the carbon content in the HIPIMS coating gradually increased from 25% at the coating substrate interface to 70% at the top thus supporting the TEM observations.

Energy-resolved mass spectrometry revealed that HIPIMS plasma is a factor of 10 richer in C^{1+} ions, and therefore more reactive, as compared to the plasma generated by standard magnetron discharge at the same conditions. The peculiar structure evolution in HIPIMS is discussed in relation to target poisoning effect and carbon outward diffusion during coating growth.

Highly abrasive AlSi9Cu1 alloy was dry machined using TiAlCN/VCN coated 25 mm diameter end mills to investigate the coating-work piece material interaction. Green (532nm excitation) and ultraviolet (325 nm excitation) Raman spectroscopy was employed to identify the phase composition of the built up material on the cutting edge and chip (swarf) surfaces produced during machining. These analyses revealed formation of lubricious Magnèli phases namely V_2O_5 and graphitic carbon as well as highly abrasive SiO_2 and mixed (AlSi)O thus shedding light on the wear processes and coating tribological behaviour during machining.

Key words: High Power Impulse Magnetron Sputtering, nanoscale multilayer, reactive sputtering.

1. Introduction:

The research and development on functional PVD coatings for cutting tools has a long history. In the early seventies technologies such as magnetron sputtering and arc evaporation were the main choice of use. In later years the Arc Bond Sputtering [1] was introduced in an attempt to combine the advantages of both sputtering (smooth coatings) and arc evaporation (high adhesion). Finally in the recent decade High Power Impulse Magnetron Sputtering (HIPIMS) was introduced [2], which after its successful up-scaling in 2003 [3] attracts growing attention as an ionised technology for coating deposition on cutting tools [4, 5].

Similarly, coatings evolved from simple single nitrides and carbides such as TiN and TiC to alloyed nitrides, carbonitrides and oxides adopting single layer, multilayer, nanoscale multilayer, nanocomposite or amorphous microstructures. Specialist coatings were developed to address the particular needs of dry high speed machining of hardened steel or machining of metallurgically reactive materials such as Al, Ti or their alloys. In the latter case two properties of the coating namely the inertness to the work piece material and the coefficient of friction turned out to be of paramount importance for the coating lifetime.

Carbon containing coatings utilising nanocomposite and nanolaminate structures have been of increased interest for the tool coating/machining industries, due to their inertness to Al-base alloys and low friction adaptability of carbon [6]. However, due to poor toughness and adhesion, state-of-the-art DLC coatings tend to fail prematurely when extreme thermal and mechanical loads are imposed during machining [7, 8]. Over-stoichiometric carbon based nanocrystalline/amorphous coatings (TiC/a-C) have also found use in low friction and wear resistance applications [9], but their poor thermal and oxidation resistance restricts wider

applicability in cutting tools/machining industries [10]. Incorporation of Vanadium has been seen as another promising alternative due to the formation of V_2O_5 a low friction Magnèli phase during sliding wear, which acts as a solid lubricant. The concept of combining V with C can be backdated to 1988, where carbon was added to Ti-Al-V-N to produce Ti-Al-V-C-N and their performance in machining was compared [11]. However, both high- and low- C containing Ti-Al-V-C-N films had shown serious adhesion and wear problems. The research in this field has led to the development of VTi (CN), [12], (TiAlV) (CNO) + V_2O_5 top layer, [13] and AlCrV (CN), [14] mainly monolithically grown or multilayer structured coatings, often with rough surfaces due to employment of cathodic arc technologies for deposition . All these coatings have shown only a moderate performance.

Recently nanostructured TiAlCN/VCN and CrAlCN/CrCN multilayer coatings deposited by the combined High Power Impulse Magnetron Sputtering (HIPIMS)/ DC magnetron Sputtering (DCMS) have shown considerable promise to protect tools at elevated temperature applications [8, 15]. These coatings have revealed the ability to adaptive self-lubrication during sliding at elevated temperatures, (700 ^{o}C) by forming variety of Magnèli phase oxides such as $AlVO_4$, Ti_nO_{2n}, V_nO_{2n} ,V_nO_{2n+1} and achieved low friction force against the work piece material [16]. In case of TiAlCN/VCN nanoscale coating, it was shown that besides the formation of Magnèli phases, carbon atoms segregated at the interfaces between the individual nanolayers changed the wear mechanism of the coating by providing low shear strength interfaces as well as reduce friction due to a graphitization mechanism taking place during sliding at elevated temperatures 300 - 700 ^{o}C [16]. Thus during the dry sliding, a unique combination of weak atomic bonding/low decohesion energy of Magnèli oxide phases and graphitic nature of carbon along with special nanolaminate layered structure of the TiAlCN/VCN coating was achieved which resulted in stabilizing the friction and wear behaviour of the coating: relatively low friction coefficient values of μ=0.45 at room

temperature which decreased to μ=0.38-0.4 at elevated temperatures, 300 - 700 ^{o}C and wear rate on the order of 10^{-17} $m^3N^{-1}m^{-1}$ at room and 10^{-15} $m^3N^{-1}m^{-1}$ at elevated temperatures. These properties have made TiAlCN/VCN coating [16] a potential candidate for applications in protective tool coatings. Indeed, we have shown that TiAlCN/VCN multilayer coating deposited by mixed HIPIMS-DCMS technology on M2 high speed steel substrates exhibit very smooth, dense microstructure, with a very high adhesion to the substrate and enhanced mechanical and tribological properties at elevated temperatures of 650 ^{o}C [17].

In the present work, we report the microstructure and functional properties of TiAlCN/VCN nanoscale coating deposited by pure HIPIMS technology. The introduction of HIPIMS in the coating deposition stage in reactive mode however requires careful consideration of the target poisoning effect. Target poisoning is an old problem in PVD technology and extensive research as well as progress has been achieved over the years in understanding, modelling and controlling the process [18, 19, 20]. However it is fair to say that the effects related to target poisoning in HIPIMS are still not very well studied and understood [21, 22]. Specifically carbon containing HIPIMS discharges have not been extensively reported. This paper attempts to shed more light on the effect of the target poisoning on the coating structure evolution, when the deposition takes place in a mixed (N_2+ CH_4) reactive atmosphere using HIPIMS. Further objective is to report on the wear mechanism and performance of the HIPIMS deposited TiAlCN/VCN when machining of Si containing Al-alloys.

2. Experimental details

2.1. Reactive deposition by HIPIMS

The TiAlCN/VCN nanoscale coating was deposited onto 30 mm diameter, 6 mm thick coupons from hardened M2 high speed steel (HRC 62) polished to Ra= 0.01 μm for mechanical and tribological characterisation. Bright annealed 304 stainless steel coupons 25 x 25 x 0.2 mm and 10 x 10 mm Silicon wafer were coated for structure analyses and surface

characterisation. The coatings were deposited in an industrial sized coating machine (HTC 1000-4 ABS manufactured by Hauzer Techno Coating, The Netherlands) enabled with HIPIMS technology at Sheffield Hallam University in UK using power supplies manufactured by Huttinger Electronic Sp. Z o.o. The coating machine with chamber volume of 1 m^3 comprises four rectangular cathodes target dimensions 200 mm x 600 mm x 15 mm. For this study, two opposing magnetrons furnished with TiAl (50:50 at%, 99.8% pure) and V (99.8% pure) targets, were operated in pure HIPIMS mode where as the other two magnetrons were shielded. A schematic cross section of the system is shown in the Figure 1. Throughout the process, the substrates were subjected to three fold rotation primary rotation speed 5 rpm. Prior to deposition, the substrate surface was bombarded by V^+ + Ar^+ ions generated from a HIPIMS discharge sustained on the V target in Ar atmosphere to pre-clean the surface for adhesion enhancement [25]. To maintain constant voltage during the ion bombardment a HIPIMS dedicated power supply manufactured by Huttinger Electronic Sp. Z o.o. was used [23]. Detailed explanation of the surface pretreatment step is described elsewhere [24, 25]. In the next step of the process, an 800 nm thick TiAlN base layer was deposited in Ar+N_2 atmosphere by operating one TiAl target in HIPIMS mode. In the final stage of the coating, methane (CH_4) gas was introduced in the vacuum chamber and deposition was carried out in a mixed Ar+N_2+CH_4 reactive atmosphere at 450°C using both targets. The flow rates of the individual gasses in this step were as follows: 180 sccm for Ar, 120 sccm for N_2 and 120 sccm for CH4. The deposition steps were carried out in ion assisted coating growth conditions of pure HIPIMS mode at total pressure of 3.10^{-3} mbar, using, 200 µs duration rectangular I-V pulses at frequency of 100 Hz .

2.2. Coating and plasma characterisation techniques

In order to characterise the plasma conditions during the deposition process as well as the mechanical, tribological, micro-structural and high temperature oxidation resistance

properties of the TiAlCN/VCN coating, several plasma and surface characterization techniques were used.

The plasma analysis has been carried out in a laboratory scale ultra- high vacuum chamber model CMS-18 (Kurt J. Lesker) equipped with 3-inch diameter targets of TiAl and V operated in HIPIMS and DCMS discharge mode. The discharge conditions such as average and peak power density and gas pressure were the same as those of the deposition experiments conducted in the industrial sized Hauzer HTC-1000-4 machine. An energy-resolved mass spectrometer PSM003 (Hiden Analytical Ltd.) was utilised to quantify the time-averaged ion composition in the plasma. The relative content of each ion was determined by integrating its corresponding ion energy distribution function. Results are interpreted by comparison between HIPIMS and DCMS in order to cancel out differences between the laboratory and industrial scale setups. In a strict sense, the lab scale experiments replicate the conditions in the industrial scale setup when the sample is in the proximity of the target whilst facing it. Experiments have shown that layer deposition occurs even when the samples are far away from the target as well.

Glancing angle X-ray diffraction (GAXRD) analysis in parallel beam geometry was used to determine the phase composition and structure of the coating as a function of the penetration depth using a Panalytical X'Pert automated diffractometer.

Auger electron spectroscopic analysis was carried out with a Physical Electronics PHI 660 instrument equipped with a LaB_6 electron gun, single pass cylindrical mirror analyzer, single channel electron multiplier and Ar ion gun for depth profiling.

Relevant cross-sections from as-deposited coatings were prepared for scanning electron microscopy using FEI NOVA-NANOSEM 200 and transmission electron microscopy (TEM) observation using a Philips CM430 instruments.

The Raman spectra were measured at room temperature using a HORIBA JOBIN YVON HR800 integrated Raman spectrometer fitted with green (λ =532nm) and UV (λ = 325 nm)

lasers. The microscope was coupled confocally to a 800 mm focal length spectrograph equipped with two switchable gratings (600 g/mm and 2400 g/mm). The 2400 g/mm grating was used for collecting the spectrum with a spectral resolution of 2-3 cm^{-1}. A 50 % transmission filter was used to reduce the intensity of incident beam. A silicon based multichannel array detector (CCD) was used to collect the output signal scattered from the samples. Utilisation of UV laser excitation allowed analysing from very thin layer (nm in thickness) from the top of film. Another advantage of utilisation of UV laser is the increased sensitivity by factor of 14 as compared to that using excitation in visible range. The Raman spectrum was acquired for 5 times in the wavelength range of 200 – 2200 cm^{-1} and 400-2000 cm^{-1} for 532nm and 325nm lasers respectively and their average was plotted. The background of the spectrum was corrected using straight line during analyses.

To determine the oxidation resistance, thermo gravimetric analysis was carried out in high performance modular Thermo Gravimetric Analyser (TGA- ambient 1750°C) from SETARAM instrumentation. The micro-balance was coupled with a maximum load of 35 g, capable temperature drift stability of 5 µg/°C and mass sensitivity of 1 µg. The TG samples (stainless steel 304 coupons with dimension 50 x 15 x 0.5 mm) were coated from all sides in order to eliminate substrate contributions during the oxidation process. Oxidation of TiAlCN/VCN coatings deposited by reactive HIPIMS was assessed by TGA in the range from room temperature to 1000°C at a linear ramp rate of 1 °C min^{-1}.

The micro hardness of the coating was measured by an MVK-H2 Mitutoyo Knoop hardness tester, with normal load of 0.25 N. To characterise the adhesion strength of the coating a CSM REVETEST scratch test analyser was used to determine the critical load, Lc (N) where the first spallation of the coating takes place.

A CSM pin-on-disc contact geometry room- and high temperature tribometers have been used to measure the friction and wear coefficient of the coated sample. Al_2O_3 balls 6 mm in diameter were used as counterparts under constant normal load of 5 N. Tests were carried out

at sliding speed of 10 ms^{-1}, at constant acquisition frequency of 1 Hz. The tests were conducted for 10000 laps at room temperature and for 2000 laps at three different elevated temperatures, (200°C, 450°C, and 650°C) in ambient atmospheric condition. A precise wear track depth profiling was carried out using a Veeco Dektak 150 instrument to generate data for calculation of the coating sliding wear coefficient.

Two flute 25 mm diameter, 2.5 mm radius high-speed machining end mills from S290 HSS material were coated with TiAlCN/VCN nanoscale multilayer coating by HIPIMS technique. The end mills were used for dry machining of wrought Al7010-T7651 alloy most frequently nowadays used in aerospace applications. The chemical compositions of work piece (Al-alloy) was wt% Cu 1.68%, Mg 2.11%, Mn 0.01%, Zn 5.92%, Fe 0.08%, Si 0.04% and rest of the composition was Al. A MAZAK FJV-25 high speed milling machine was used to carry out this test. The spindle speed 24000 rpm, cutting speed Vc of 1884 m min^{-1} was set as milling test parameter. The feed rate Vf = 0.165 mm per tooth (0.33 mm rev^{-1}) with cutting depth Ap and cutting width Ae of 4 mm and 2 mm respectively was achieved during the machining. Raman spectra were collected from tool edge after certain interruptions at regular times.

3. Results and Discussions

3.1. Plasma Compositional Analysis

Ion composition determined by mass spectrometry is shown in Figure 2. The results were recorded for conditions corresponding to coating deposition of TiAlCN and VCN which constitute the TiAlCN/VCN nanoscale multilayer. During plasma analysis of the deposition of individual layers carried out in the laboratory scale machine the average power density and total pressure (including partial pressure of the individual gases) were the same as for the deposition of nanoscale multilayers in the industrial scale setup.

Figures 2a and 2b, show the results for the deposition of the TiAlCN layer in HIPIMS and DCMS modes respectively. The metal ion content in the HIPIMS discharge was about 12% with Al^{1+}=9%, Ti^{1+}=2%, and C^{1+}=1%. In DCMS mode, we detected factor 4 lower metal ion content of ~3% distributed among: Al^{1+}= 2.8%, Ti^{1+}= 0.23% and C^{1+}=0.13%. The ion flux in both processes was dominated by gas. Ions of the following gaseous species were identified in mass spectra: Argon, N_2, stable hydrocarbons (CH_4, C_2H_2, C_2H_4, C_2H_6, C_3H_8), radicals (CH, CH_2, CH_3, C_2H, C_2H_5, C_3H_2, C_3H_3, C_3H_6, C_3H_7), and nitril compounds (HCN, H_2CN, NH, and NH_3). The total gas ion content was about 88% of the plasma in the case of HIPIMS and about 97% in the case of DCMS discharge.

Likewise, Figures 2c and 2d show the plasma composition during the deposition of VCN by HIPIMS and DCMS respectively. The metal ion concentration was found to be 7.73% in case of HIPIMS and significantly lower at 0.56% in case of DCMS discharge. It is important to note that free C^{1+} ions were found at 4 time higher concentration in HIPIMS than DCMS. Meanwhile, about 91.78% and 99.26% of gas ions were detected during HIPIMS and DCMS discharge respectively. The ratio of metal ion-to-gas ion concentration during HIPIMS deposition was 1:7 and 1:12 for TiAlCN and VCN respectively. These ratios are significantly lower in DCMS deposition with 1:32 for TiAlCN and 1:177 for VCN.

The obtained results about gaseous ion species in the discharge are consistent with published experimental results and chemical models obtained for similar plasmas [26, 27, 28].

During the HIPIMS deposition step, high current densities applied in pulses are believed to stimulate several processes inside the active plasma, such as electron impact excitation of metastable N_2*, excitation of atomic nitrogen and formation of free radicals [26], which are efficient to dissociate methane (CH_4) into several gaseous ions of hydrocarbons, and nitrils [26, 27, 28] in the Ar+N_2+CH_4 plasma. The high frequency of electron impacts produces stable free carbon ions of C^{1+} [28]. In HIPIMS the latter process is much more efficient compared to DCMS.

The metal and carbon ions detected during deposition influence the coating growth in several aspects. For example enhanced metal ion bombardment during HIPIMS deposition will densify the microstructure by reducing intercolumnar porosity. Furthermore it can promote layer-by-layer growth and reduce the roughness of the coatings.

High amounts of free carbon produced in the HIPIMS plasma itself tend to enhance the incorporation of carbon in the actual film. In contrast C_xH_y molecules and radicals have lower sticking coefficients and/or may require additional energy to dissociate on the surface.

The various ionised reactive gas species bombard the target during sputtering and are expected to intensify chemical reactions on the surface.

3.2. Coating structure characterisation by GAXRD

In the present work, glancing angle (GA) measurements were performed at incidence angles of 1^o, 2^o, 5^o and 10^o; the diffraction patterns are shown in Figure 3. The structure was found to be a single phase *fcc* structure (NaCl) and resolving individual reflections from the TiAlCN and VCN phases was not possible. Depending on the incidence angle the shape of the diffraction peaks changes from broader and lower intensity peaks at small angles, (1^o, 2^o) to sharper and higher intensity peaks as well as additional reflection from {311} and {222} planes at 5^o and 10^o. This is confirmed by full-width at half-maximum (FWHM) measurements where the values for the (111) reflection change from 2.77^o at 1^o to 1.55^o at 10^o. GAXRD characterisation indicates that the structure of the coating gradually changes with thickness from larger grain crystalline at the base to random orientation smaller grain nanocrystalline to almost X-ray amorphous structure at the top. In fact the 1^o GA pattern is very similar to the previously discussed by the authors [29] patterns taken from Cr-C coatings where the carbon content exceeds 80%, which sheds further light on the nature of the top 0.360 μm of the film.

3.3. Structure evolution of TiAlCN/VCN nanoscale coating deposited by HIPIMS

Figure 4(a) shows the fractured cross-sectional SEM micrograph of TiAlCN/VCN coating deposited on silicon wafer using pure HIPIMS technology. The micrograph reveals the columnar structure of the coating with three distinct zones. The adjacent to the substrate first zone is the carbon free (TiAlN) base layer which shows highly dense small diameter (~60nm) columns terminated with flat tops. This is followed by a narrow dark band (~250nm) where no structural features can be observed under SEM, second zone. The third zone represents the bulk of the coating consisting larger diameter (~180 nm) columns. The columns are slightly wider on the top but no structural features associated with competitive growth mechanism can be clearly observed. Interestingly the columns have a peculiar granular, (cauliflower like) structure which can be clearly seen on the micrograph taken at higher magnification, Figure 4b. In the case of pure HIPIMS deposition the coating growth is influenced by two factors, these being the carbon segregation and enhanced ion bombardment, which result in formation of the observed intra-columnar structure. In comparison when the same coating is deposited using DSCM process an open, broken-rock like coarse columnar structure is observed Figure 4c. Most of the columns are terminated with a horizontal terrace, which indicates relatively weak interface bonding between the individual layers of the nanolaminated material. Another difference in the cross section structures between pure HIPIMS and DCMS is the absence of the zone two (featureless dark band) for the coating produced by the DCMS process.

Cross-sectional TEM imaging revealed further details of the fine structure of the HIPIMS deposited TiAlCN/VCN. Figure 5a is a low magnification BF image, which shows the structure of the main coatings areas such as TiAlN base layer followed by uniform gray contrast narrow band, followed by area with columnar structure where the column boundaries are decorated with a white phase based on a light atomic weight element. Previous research

on nanoscale multilayer structured TiAlCN/VCN coatings deposited by DCMS techniques employing HRTEM and STEM-EELS analyses have shown that the white phase is carbon, which accumulates at the interfaces of the individual nano layers during growth of the laminated structure as well as at the column boundaries [30]. Column boundary segregation has been also observed for single layer TiAlCN reported elsewhere [31]. The location of the narrow grey contrast band adjacent to the base layer corresponds to the zone two of the SEM cross section, see Figure 4a. Higher magnifications revealed further details of the coatings architecture, Figure 5b. A nanoscale multilayer structure with bi-layer thickness of 5-8nm and total thickness of 30nm can be observed right above the TiAlN base layer. This is believed to correspond to zone two of the cross section SEM and the grey contrast band in the low magnification TEM image, Figure 5a. Careful observation reveals a white lateral phase segregated at the interfaces of the individual layers. This structure is typical for TiAlCN/VCN coatings deposited by sputtering and its growth mechanism was described previously in [30]. The structure which evolves further with coating growth (Figure 5b) is one of a typical nanocomposite consisting of dark contrast grains surrounded by carbon-based phase forming a white contrast tissue phase. The nanograins - marked with arrows in Figure 5b - are most probably MeCN where Me is Ti-Al-V. The largest grains with diameter in the range of 5-10 nm are formed right after the band with nanoscale multilayer structure. As growth progresses the size of the grains gradually reduces until an amorphous phase forms at the surface of the coating. Figure 6 is a High Resolution TEM micrograph showing the nanocrystalline grains (some marked with arrows) and the surrounding tissue phase structure.

The grain size reduces gradually with thickness at the expense of the white phase and no grains can be seen on the very top region of the coating. Selected Area Electron Diffraction (SAED) analyses were carried out in different zones of the coating namely base layer and nanoscale multilayer, bulk of the coating and top of the coating, Figure 7 a, b, c. The analyses showed that a gradual transformation in the structure with thickness of the coating takes place

changing from crystalline at the base to nanocrystalline in the bulk and finally random orientation small grain nanocrystalline to almost X-ray amorphous structure on the top thus confirming the GAXRD findings and providing further information for better understanding and interpretation of the XTEM results.

This unique structure and obviously compositional evolution obtained in one deposition process is believed to be due to the target poisoning effect which takes place in reactive (carbon-nitrogen containing atmosphere) HIPIMS. A clear evidence about the reactivity of the HIPIMS plasma sustained in a mixed CH_4+N_2+Ar atmosphere was gathered by the energy resolved mass spectrometry, see paragraph 3.1. The large amount and variety of reactive gas ions as well as free carbon ions (C^+) influences strongly both the target poisoning effect (reduction of the metal content in the film with time) as well as the C incorporation in the film. AES depth profile, Figure 8 revealed that the C content in the film gradually increased with the film thickness from 25 at % at the TiAlN base layer-TiAlCN/VCN coating interface to 70% at the very top of the coating.

3.3. Oxidation resistance by Thermo Gravimetric analysis:-

Figure 9 shows the results from TG oxidation analyses of TiAlCN/VCN coating deposited by reactive HIPIMS technique on stainless steel substrates. For comparison, TG curves obtained for the same coating deposited by conventional DCMS and mixed HIPIMS+DCMS (two cathodes in HIPIMS and two cathodes in DCMS operated simultaneously) techniques were also presented. All measurements wear performed with linear temperature ramp at 1^oC/min from room temperature to 1000 ^oC. Significant difference can be seen in the case of reactive HIPIMS deposited TiAlCN/VCN coating. The onset of rapid oxidation was shifted to higher temperatures of about ≈ 810 ^oC as compared to the DCMS and HIPIMS+DCMS cases. Furthermore, compared to the DCMS deposited coatings, no significant oxidation at 550°C was observed. The weight gain due to oxidation is lower by factor of two when compared to

DCMS deposited TiAlCN/VCN coating which again demonstrates the effect of the coating densification due to utilisation of HIPIMS.

3.4. Mechanical and tribological properties of TiAlCN/VCN coating deposited by reactive HIPIMS:

TiAlCN/VCN coatings deposited by reactive HIPIMS technology showed high microhardness values of 2700 $HK_{0.025}$. The adhesion strength was evaluated by determination of the critical load value using scratch test. Repeatedly high Lc=55N values were measured for this type of coating independent from the deposition method, DCMS, mixed HIPIMS+DCMS and pure HIPIMS provided that the surface pretreatment was carried out by HIPIMS V^+ ion bombardment [17, 25].

Friction and Wear behaviour of the coating at room and elevated temperatures:

Coating friction and wear behaviour at room and elevated temperatures was investigated by pin-on-disc tests using Al_2O_3 counterpart. Figure 10a shows the friction curve at room temperature depicting the "running" stage and beginning of the "steady state" of the dry sliding process. Here one can clearly distinguish between two friction zones. Immediately after the "running" stage the friction curve changes its slope indicating the beginning of the first lower coefficient of friction zone where the mean value of μ=0.37. After that the friction gradually increases to reach a "steady state" where higher coefficient of friction values (μ=0.48) were recorded. In an attempt to "depth profile" the friction and wear behaviour of the HIPIMS deposited TiAlCN/VCN coatings a number of friction tests were carried out with stepwise increase of the sliding distance by changing the number of the sliding laps from 500 to 10000 with an increment of 1000 laps. In this experiment it was found that the wear coefficient reduces by one order of magnitude with the wear depth, with initial value of K_c = 3.8 x 10^{-15} $m^3N^{-1}m^{-1}$after 500 laps to K_c = 4.4 x 10^{-16} $m^3N^{-1}m^{-1}$after 10000 laps. In comparison, DCMS deposited TiAlCN/VCN coatings tested under similar conditions show an

order of magnitude higher wear coefficient of 4.1 x 10^{-15} $m^3N^{-1}m^{-1}$ [17] thus demonstrating the beneficial effect of the HIPIMS process. This peculiar wear behaviour is believed to result from the graded coating phase and micro structures, see paragraph 6. Coefficient of friction values of μ=0.37 as measured in the first friction zone at the top of the coating are typical for Me-DLC coatings which corresponds well to the Me-C phase and XRD amorphous structure of the coating in this area. Low friction in this stage is achieved due to the C, which acts as a solid lubricant. When the sliding distance /wear depth is increased the nanocomposite structure of the coating is reached which characterises with higher coefficient of friction compared to the C-rich top layers and enhanced wear resistance, which is expected when accounting for the higher hardness of the nanocrystalline structures. In this region the friction and wear behaviour are determined by the interplay between two mechanisms the presence of C acting as solid lubricant and formation of highly lubricious V_2O_5 Magnèli phases.

The friction behaviour of the HIPIMS deposited TiAlCN/VCN films at elevated temperatures is characterised by initial increase of COF to μ = 0.8 at 200 ^oC followed by reduction to μ = 0.45 at 650 ^oC, Figure 10b. This phenomenon is well understood and discussed in details elsewhere in [32]. The initial increase of COF is attributed to the elimination of the lubricious effect of the humidity over the sliding surface with heating where as the subsequent reduction at elevated temperatures is attributed to the formation of a range of lubricious oxides such as Ti_nO_{2n-1}, V_nO_{2n-1}, V_nO_{3n-1} or V_nO_{3n-2} due to the combined thermal and tribo-oxidation. Despite their low coefficient of friction the mechanical strength and therefore wear resistance of the oxide films is not very high, which can be seen from the increase of the wear coefficient when compared to the room temperature wear conditions. Coating densification however reduces significantly the amount of the thermally grown oxides as revealed by the TG analyses, Figure 9 which explains the superior performance of the HIPIMS TiAlCN/VCN coatings, (Kc = 1.0 x 10^{-13} $m^3N^{-1}m^{-1}$) over the DCMS deposited ones (Kc = 5.8 x 10^{-13} $m^3N^{-1}m^{-1}$) when tested at 650 ^oC.

3.5. Raman spectroscopy investigation of the warn tool-work piece material surfaces

To study the wear behaviour of TiAlCN/VCN as well as coating work-piece material interaction a cutting experiment was conducted. Coated 25 mm diameter three-flute cemented carbide end mills were used to machine highly abrasive AlSi9Cu1 alloy in dry conditions. The tests were carried out on a high-speed milling centre, MAZAK FJV-25 using milling parameters which were specifically set to produce significant amount of built up material on the cutting edge and therefore guarantee full scale coating-work piece material reaction: spindle speed; 24000 rpm; cutting speed, Vc=1884 m. min^{-1}; cutting depth, Ap=4 mm; cutting width, Ae= 2 mm; feed rate, Vf=0.165 mm per tooth (0.33 mm rev^{-1}). SEM image of the cutting tool with the built up Al-alloy on the cutting edge is shown in Figure 11a. This built up material was then mechanically removed from the tool and the contact surface, dark contrast area shown in Figure 11b was used for Raman analyses. Green (532 nm excitation) and UV (325 nm excitation) Raman spectroscopy was employed to identify the coating phases and compounds formed on the cutting edge before and after the machining test as well as on the contact surface of the as removed from the cutting edge built up material, Figure 12a and b.

As deposited coating: Both Green and UV excitations of the as deposited coating revealed the presence of TiAlCN and VCN as expected. However the more sensitive to carbon UV analyses showed, lower intensity peaks at 1568 cm^{-1} (G-band) and 1351 cm^{-1} (D-band) revealing the graphitic nature of the very top layers of the coating material, which supports the GAXRD and XTEM analyses.

Coating on the tool surface after machining: Green laser Raman spectroscopy carried out on the tool surface after the cutting test identified the presence of various oxides such as SiO_2, mixed (AlSi)O, V_2O_5 as well as the G and D bands of graphitic carbon. The graphitic G and D bands at 1372 cm^{-1} and 1605 cm^{-1} respectively were much more intensive in the UV 325nm

spectra. It is important to note that the observed in the pin-on-disc- dry sliding experiment formation of the lubricious Magnèli phase, V_2O_5 [17] takes also place in metal cutting conditions thus confirming the beneficial effect of the V in the coating in friction reduction. Apparently introducing carbon in the coating to deposit TiAlCN/VCN further influences tool surface-work piece material friction. The higher intensity D and G bands observed in both Green and UV laser spectra demonstrate that during machining graphitic carbon is formed on the coating surface which acts as a solid lubricant. The graphitisation process is believed to develop due to the combined mechanical and thermal load exerted on the tool surface during cutting. The high hardness SiO_2 and mixed (AlSi)O constitute the built up material which is "cold welded" to the tool surface. The periodic removal of this material which carries away some portions of the coating, (see Figure 11b, the dark contrast area) represents one of the wear mechanisms taking place on the cutting edge another being the micro abrasion.

Tool-chip contact area: The compounds found on the contact surface of the built up SiAl-alloy were similar to those found on the tool surface after the machining test namely lubricious V_2O_5, abrasive SiO_2 and mixed (AlSi)O, as well as graphitic carbon. This demonstrates that the material removal by cutting is accompanied by intensive material transfer between the surfaces of the tool and work piece material in the sliding contact. While this is a common situation in any cutting process this study shows that a proper coating material selection in the coating design stage could dramatically influence the tribology in the contact area by providing compounds with lubricious properties in dry sliding conditions.

4. Conclusions:

- The analyses showed that with HIPIMS grown TiAlCN/VCN a gradual transformation in the structure with thickness of the coating takes place. The structure evolves from crystalline nanoscale multilayer of TiAlCN/VCN at the base to nanocomposite structure comprising nanocrystalline TiAlVCN surrounded by C-based tissue phase in the bulk and

finally to X-ray amorphous structure of Me-C on the top. This unique structure and compositional evolution obtained in one deposition process is believed to be due to the target poisoning effect which takes place in HIPIMS in reactive (carbon-nitrogen) atmosphere.

- "Depth profiling" the friction and wear behaviour at room temperature of the HIPIMS deposited TiAlCN/VCN coatings revealed that immediately after the "running" stage, a low friction coefficient zone exists where the mean value of COF is $\mu = 0.37$. After that the friction gradually increases to reach a "steady state" zone where higher coefficient of friction value of $\mu = 0.48$ was recorded. The wear coefficient reduces by one order of magnitude with wear depth, with initial value of $K_c = 3.8 \times 10^{-15}$ $m^3N^{-1}m^{-1}$ after 500 laps to $K_c = 4.4 \times 10^{-16}$ $m^3N^{-1}m^{-1}$ after 10000 laps. In comparison, UBM deposited TiAlCN/VCN coatings tested under similar conditions show an order of magnitude higher wear coefficient of 4.1×10^{-15} $m^3N^{-1}m^{-1}$. This peculiar wear behaviour is believed to result from the combined effects of the grading of the coating microstructure and densification through the HIPIMS process.

- TG analyses revealed that the onset of rapid oxidation for reactive HIPIMS deposited TiAlCN/VCN coatings was shifted to higher temperatures of about 810 ^oC as compared to the DCMS and HIPIMS+DCMS cases. The weight gain due to oxidation was factor of two lower than DCMS deposited TiAlCN/VCN coating, which again demonstrates the beneficial effect of HIPIMS for coating densification.

- High temperature pin-on-disc tests revealed that the COF of HIPIMS-deposited TiAlCN/VCN initially increases to $\mu = 0.8$ at 200 ^oC and then decreases to $\mu = 0.45$ at 650 ^oC. Owing to their denser microstructure and enhanced oxidation resistance, HIPIMS deposited TiAlCN/VCN show superior performance at elevated temperatures of 650 ^oC, ($K_c = 1.0 \times 10^{-13}$ $m^3N^{-1}m^{-1}$) over the DCMS deposited ones ($K_c = 5.8 \times 10^{-13}$ $m^3N^{-1}m^{-1}$).

- The cutting edge of TiAlCN/VCN coated end mills and the contact surface of the built up material produced during machining of Al-Si alloy were studied successfully by Raman spectroscopy. The analyses revealed that the cutting process produces highly abrasive phases

of SiO_2 and mixed (AlSi)O, which produce considerable wear of the cutting edge. However, the presence of lubricious V_2O_5 - Magnèli phases formed via tribooxidation and graphitic carbon formed via high temperature exposure and mechanical impact is expected to significantly reduce the negative affect of the above mentioned abrasive phases on the cutting edge life time.

4. References

[1] W.-D. Münz, D. Schulze, and F.J.M.Hauzer, Surf. Coat. Technol. 50 (1992) 169.

[2] V. Kouznetsov, K. Macak, J.M. Schneider, U. Helmersson, I. Petrov, Surf. Coat. Technol. 122 (2–3) (1999) 290.

[3] A.P. Ehiasarian and R. Bugyi, *Industrial Size High Power Impulse Magnetron Sputtering*, (Proceedings of the 47th Annual Technical Conference of the Society of Vacuum Coaters, Dallas, TX, United States, 2004), 437 (2004)

[4] M. Eerden, F. Papa, T. Krug, D. Driesenaar, Vakuum in Forschung und Praxis 24 (1) (2012) 6.

[5] O. Lemmer, W. Kölker, S. Bolz, C. Schiffers, IOP Conf. Ser.: Mater. Sci. Eng., 39 (1) (2012) 012003.

[6] M. Lahres, P. Müller-Hummel, O. Doerfel, Surf. Coat. Technol. 91 (1997) 116.

[7] A.A. Voevodin, J.S. Zabinski, Compos. Sci. Technol. 65 (2005) 741.

[8] P. Eh. Hovsepian, A. P.Ehiasarian, A. Deeming, C. Schimpf, Vacuum, 82 (2008) 1312.

[9] Y.T. Pei, D. Galvan, and J.T.M. De Hosson, Materials Science Forum 475-479 (2005) 3655.

[10] S. Veprek, M. G. J. Veprek-Heijman, P. Karvankova, J. Prochazka, Thin Solid Films 476 (2005) 1.

[11] O. Knotek, M. Atzor and H.-G. Prengel, Surf. Coat. Technol. 36 (1988) 265.

[12] T. Yusuke, Kobe Steel, JP4221057 (1990).

[13] O. Hisanori at al. Sumitomo Electric Industries, JP 32406797 (1996).

[14] K. Yamamoto at al. Kobe-Steel, US2003/0148145 A1, (2003).

[15] P. Eh. Hovsepian, A. P. Ehiasarian, U. Rataysaki, Surf. Coat. Technol. 203 (2009) 1237.

[16] G. Kamath, A. P. Ehiasarian, P. Eh. Hovsepian, Surf. Coat. Technol. 205 (8-9) (2011) 2823.

[17] G. Kamath, A. P. Ehiasarian, P. Eh. Hovsepian, IEEE Trans. Plasma Sci. 38 (11) (2010) 3062.

[18] S. Berg, H.-O. Blom, T. Larsson, C. Nender, J. Vac. Sci. Technol. A 5 (2) (1987) 202.

[19] D. Depla R.De Gryse, Surf. Coat. Technol. 183 (2004) 184; 183 (2004) 190; 183 (2004) 196.

[20] D. Güttler, B. Abendroth, R. Grötzschel, and W. Möller, Appl. Phys. Let. 85 (25) (2004).

[21] E. Wallin and U. Helmersson, Thin Solid Films, (516), 18 (2008), 6396.

[22] M. Andronis, V. Bellindo-Gonzalez, Thin Solid Films, Vol.518, 1962-1965, (2010).

[23] A. P. Ehiasarian, R. Tietema, P. Hovsepian, D. Doerwald, R. Bugyi, A. Klimczak, ZL200780012990.9 in China, granted 10.04.2011, priority 10.04.2007.

[24] A. P. Ehiasarian, P. Eh. Hovsepian, W.-D. Münz, EP 1 260 603 A2.

[25] A. P. Ehiasarian, J. G. Wen and I. Petrov, J. Appl. Phys. 101 (5) (2007).

[26] C.D. Pintassilgo, J. Loureiro, G. Cernogora and M. Touzeau, Plasma Sources Sci.

Technol. 8 (1999) 463.

[27] C. D. Pintassilgo, J. Loureiro, Planetary and Space Science 57 (2009) 1621.

[28] J. C .Legrand, A. M. Diamy, R. Hrach, V. Hrachova, Vacuum 48 (1997) 671.

[29] Y. N. Kok, P. Eh. Hovsepian, Q. Luo, D. B. Lewis, J. G. Wen, I. Petrov, Thin Solid Films 475 (2005) 219.

[30] P. Eh. Hovsepian, A. P. Ehiasarian, I. Petrov, Surf. Engin. 26 (2010) 610, DOI 10.1179/026708408X336337.

[31] M. Stueber, C. Ziebert, H. Leiste, S. Ulrich, C. Sanz, E. Fuentes, I. Etxarri, M. Solay, A. Garcia, P. B. Barna, and P. Hovsepian, Machining Science and Technology, 13:122–141, DOI: 10.1080/10910340902782687.

[32] Z. Zhou, W. M. Rainforth, Q. Luo, P. Eh. Hovsepian, J. J. Ojeda, M. E. Romero-Gonzalez, Acta Materialia 58 (2010) 2912-2925.

6. List of figure captions

Figure 1. Schematic cross-section of the four cathodes of the HTC 1000-4 PVD coating system.

Figure 2. Mass spectrometer study of the plasma composition in HIPIMS and DCMS discharge a) and b) for TiAlCN, c) and d) for VCN.

Figure 3. GA X-ray diffraction patterns taken at various incidence angles

Figure 4. SEM cross-sectional view of TiAlCN/VCN nanoscale coating deposited by reactive HIPIMS deposition (a) lower magnification coating cross-section (b) higher magnification coating cross-section (c) lower magnification coating cross-section for coating deposited by DCMS process.

Figure 5. Bright field TEM cross-section of TiAlCN/VCN nanoscale coating deposited by reactive HIPIMS deposition (a) lower magnification coating cross-section (b) higher magnification coating cross-section.

Figure 6. HRTEM micrograph of the zone with nanocomposite structure of TiAlCN/VCN

Figure 7. SAED patterns taken from various coating zones: a) TiAlN base layer/ nanoscale multilayer zone, b) nanocomposite zone, c) top of the coating.

Figure 8. AES depth profile showing a gradual increase of C concentration with film thickness suggesting a target poisoning effect.

Figure 9. Thermo gravimetric oxidation rate measurement using a linear ramp at 1 ^{o}C min^{-1} for reactive HIPIMS deposited TiAlCN/VCN coating.

Figure 10. Coefficient of friction curves (μ), versus number of laps for reactive HIPIMS deposited TiAlCN/VCN coating: a) room temperature test, b) elevated temperature test.

Figure 11. Three-flute cemented carbide end mill coated with TiAlCN/VCN : a) overall view showing the built up layer on the cutting edge after dry machining of AlSi9Cu1alloy, b) image of the built-up material detached from the cutting edge.

Figure 12. Raman spectra taken from various surfaces using: a) UV, 325 nm excitation and b) green laser 532 nm excitation.

7. Figures

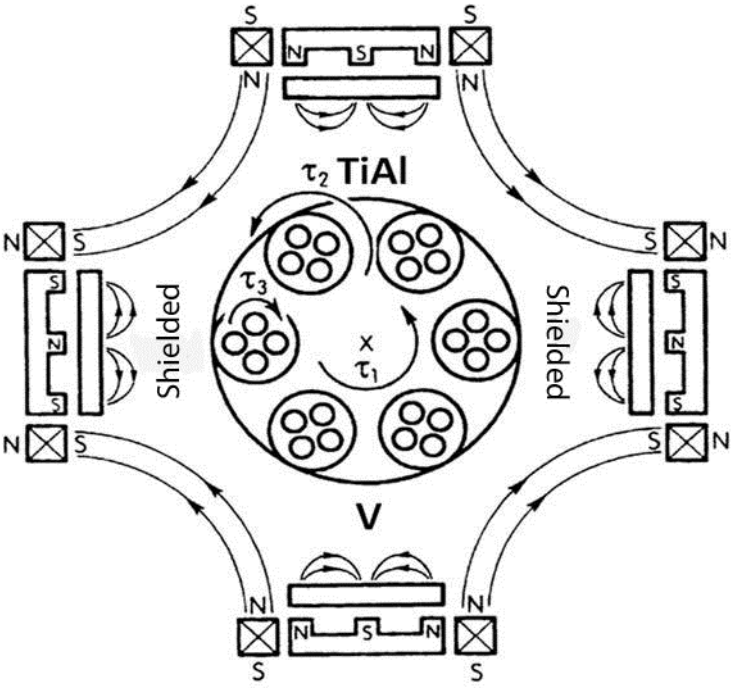

Figure 1.

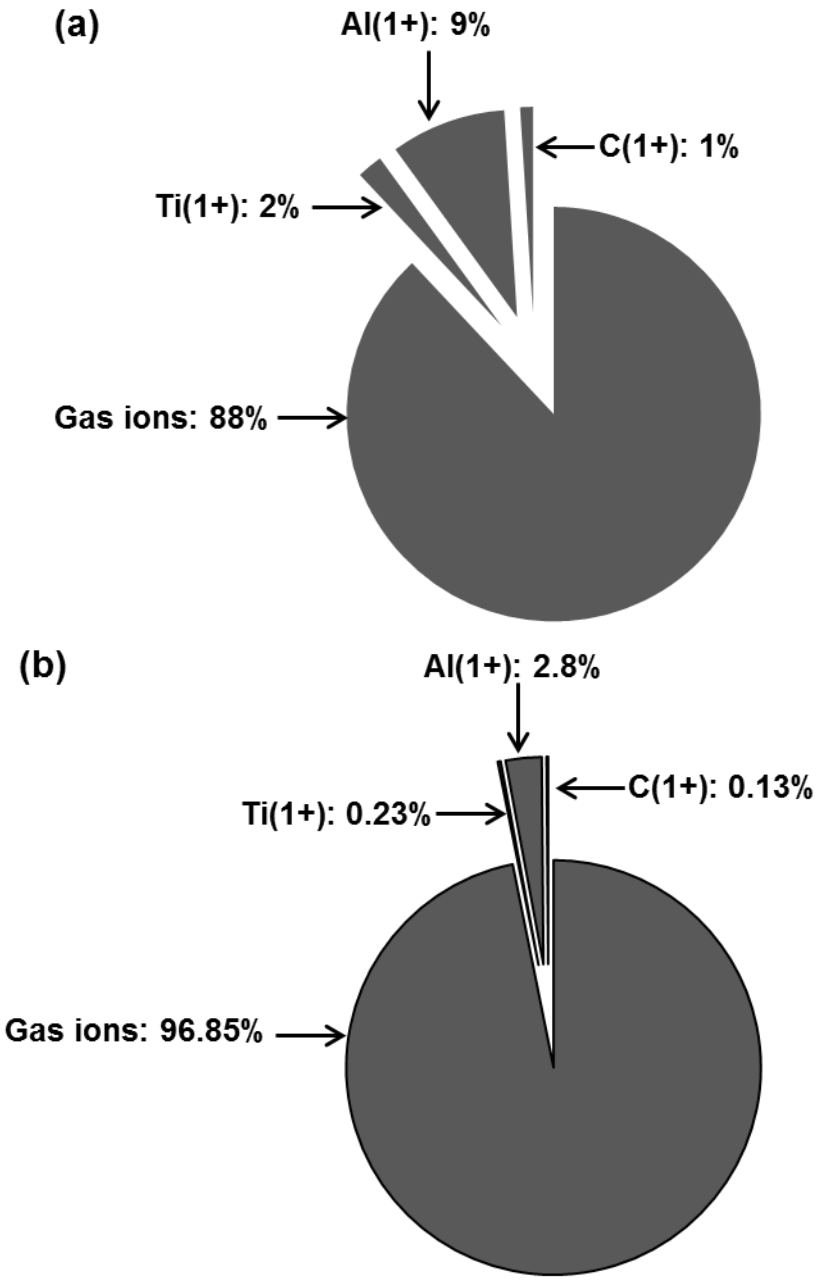
(a)
Al(1+): 9%
C(1+): 1%
Ti(1+): 2%
Gas ions: 88%
(b)
Al(1+): 2.8%
C(1+): 0.13%
Ti(1+): 0.23%
Gas ions: 96.85%

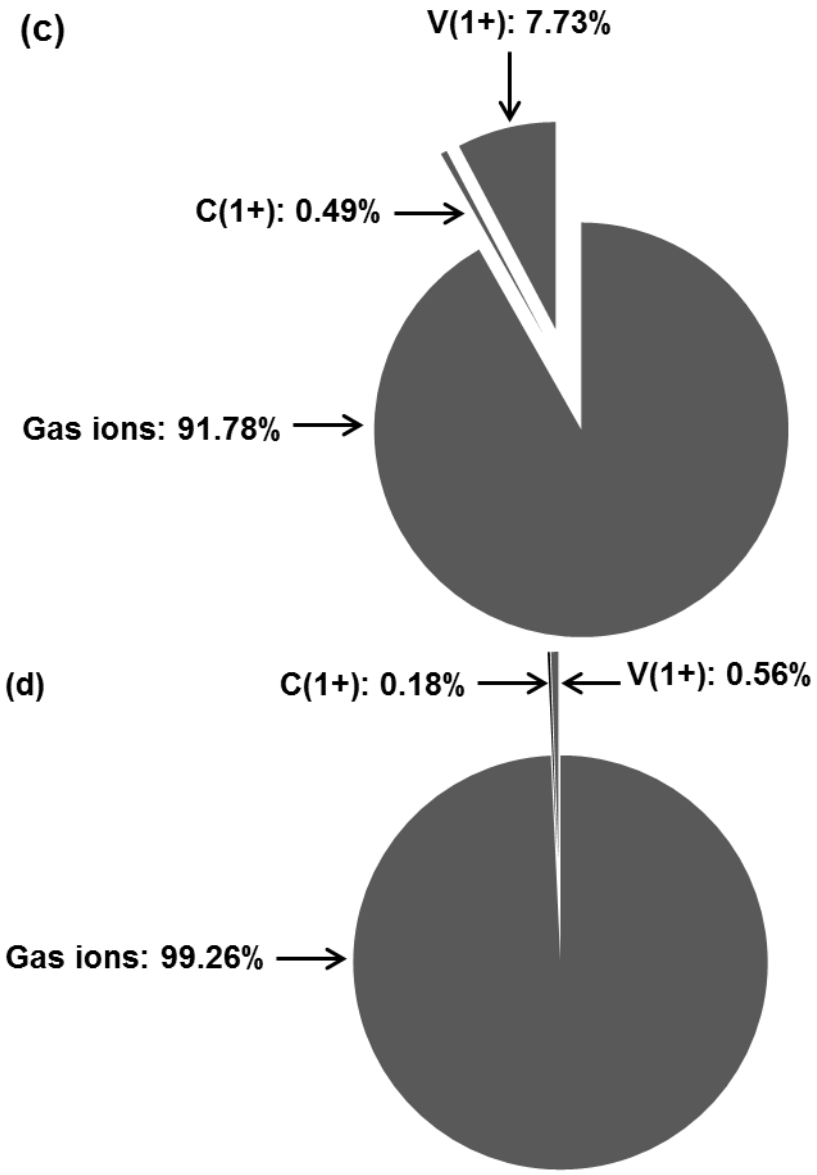

Figure 2.

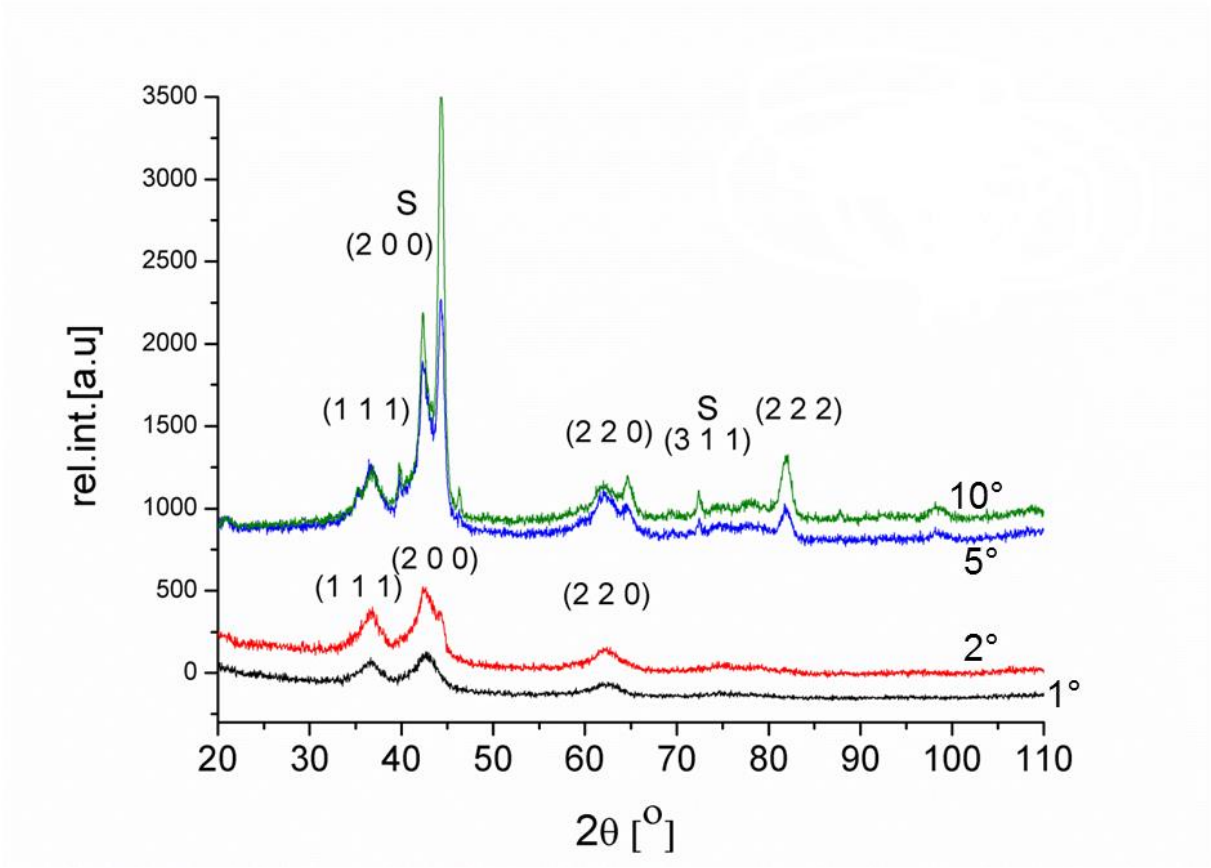

Figure 3.

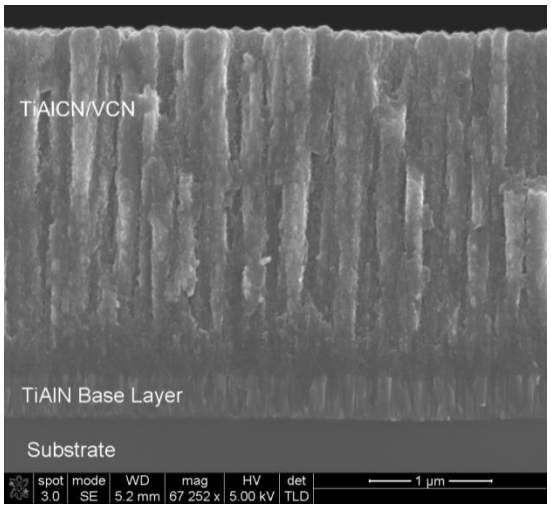

Fig. 4a

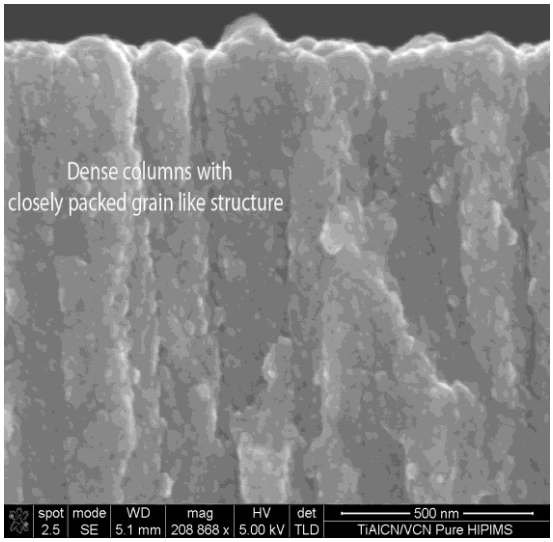

Fig.4b

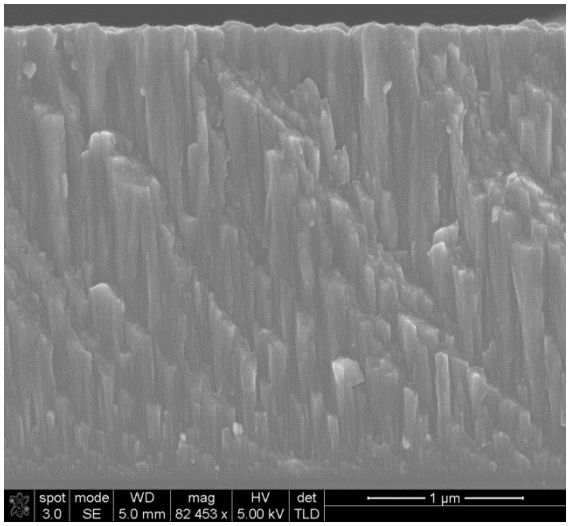

Fig.4c

Figure 4.

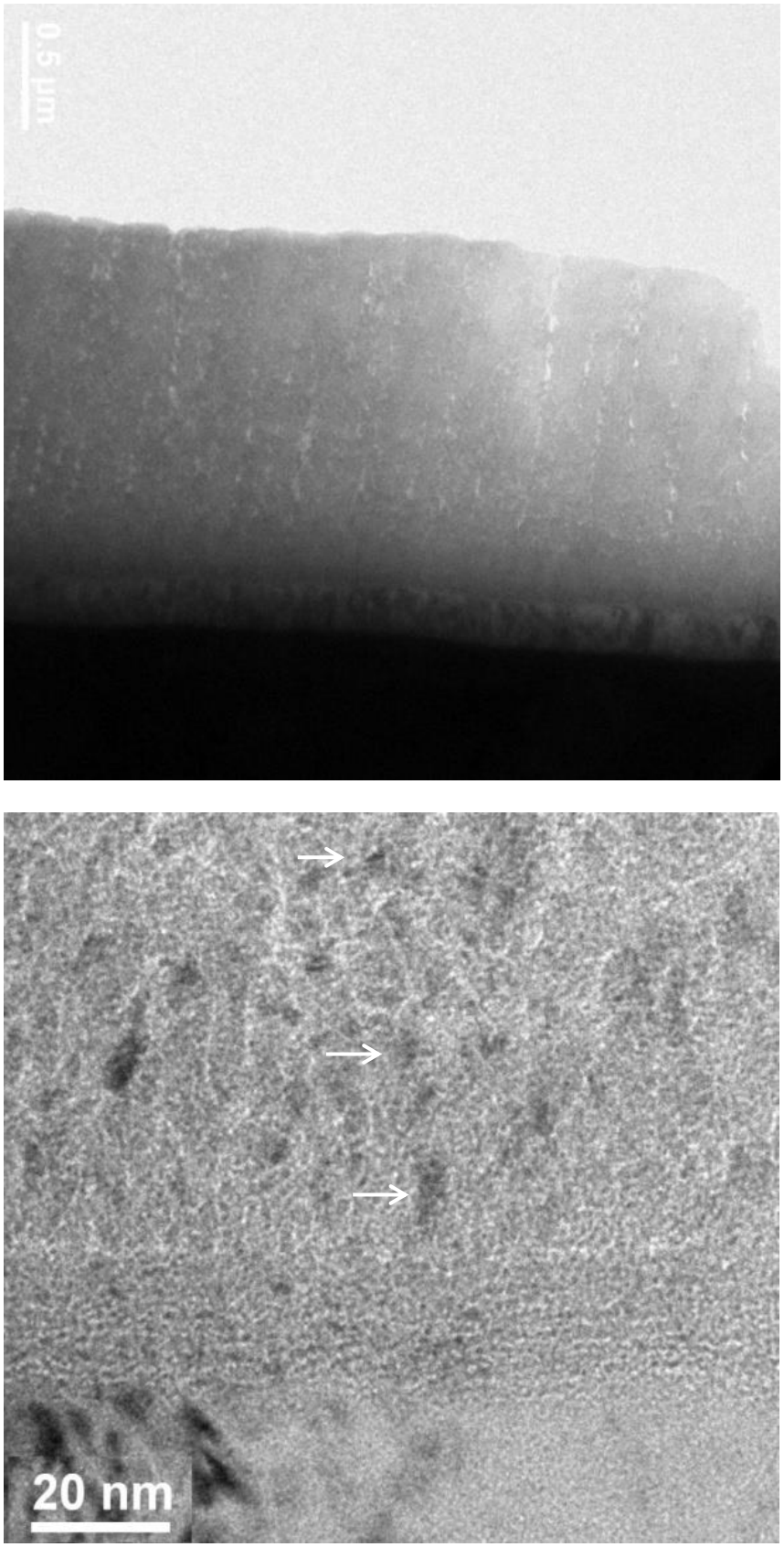

Figure 5

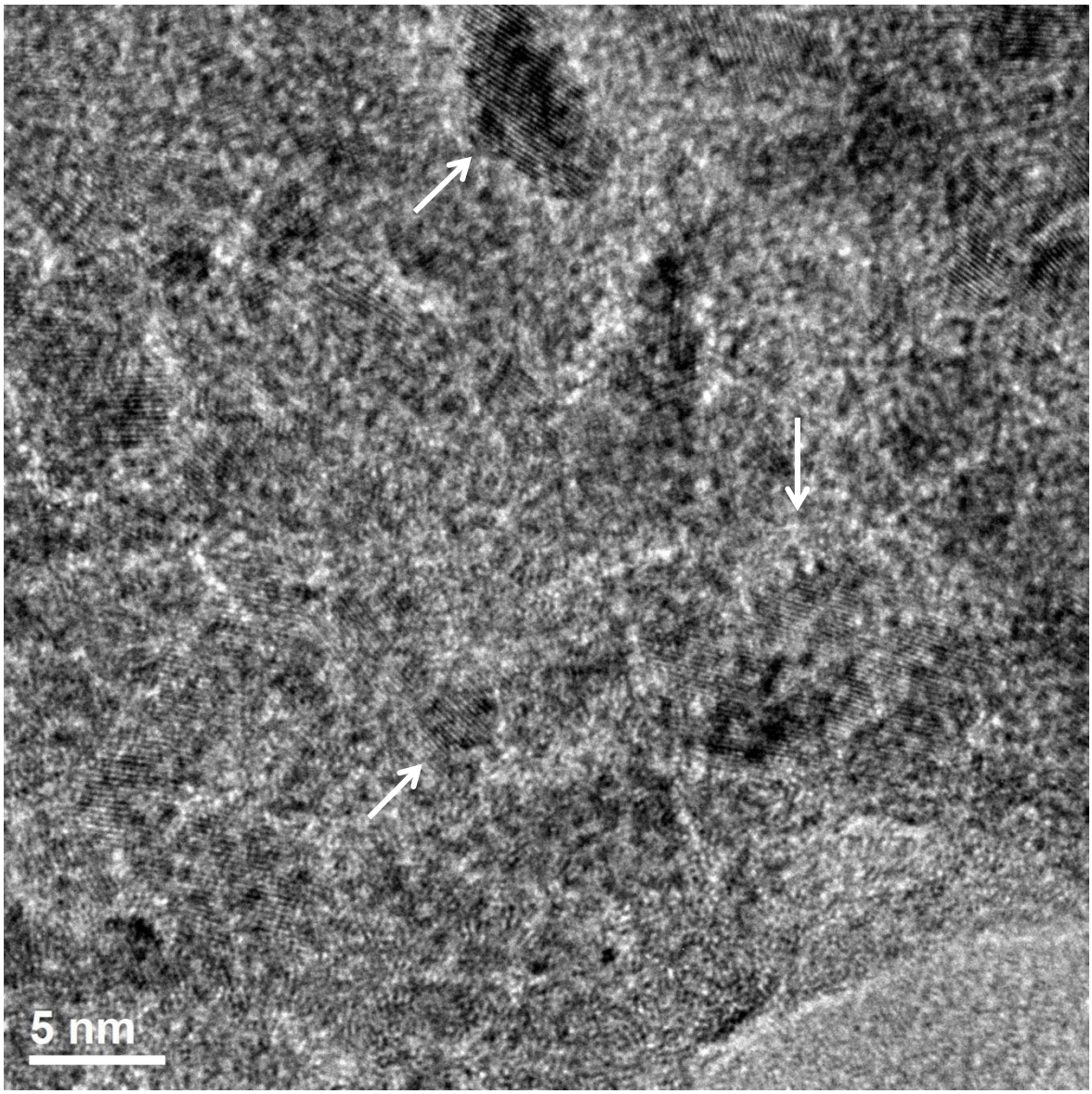

Figure 6

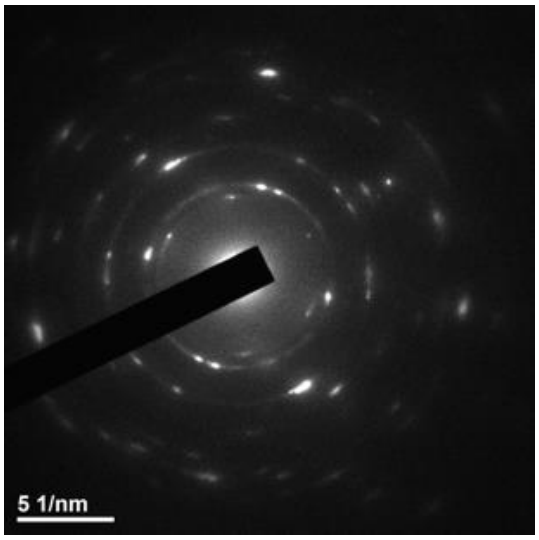

Figure 7a

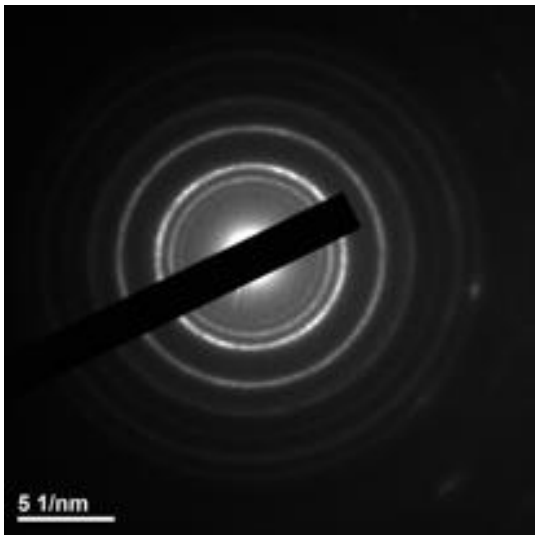

Figure 7b

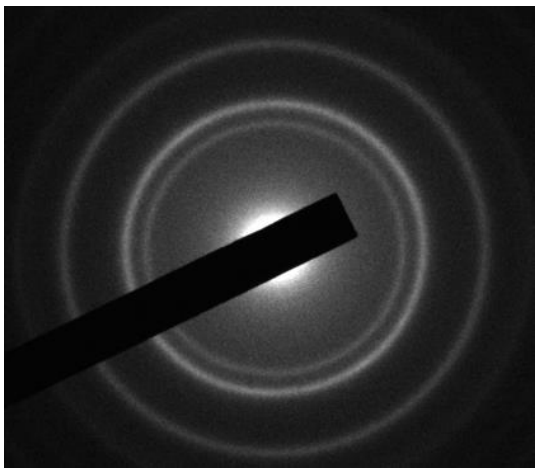

Figure 7c

Figure 7

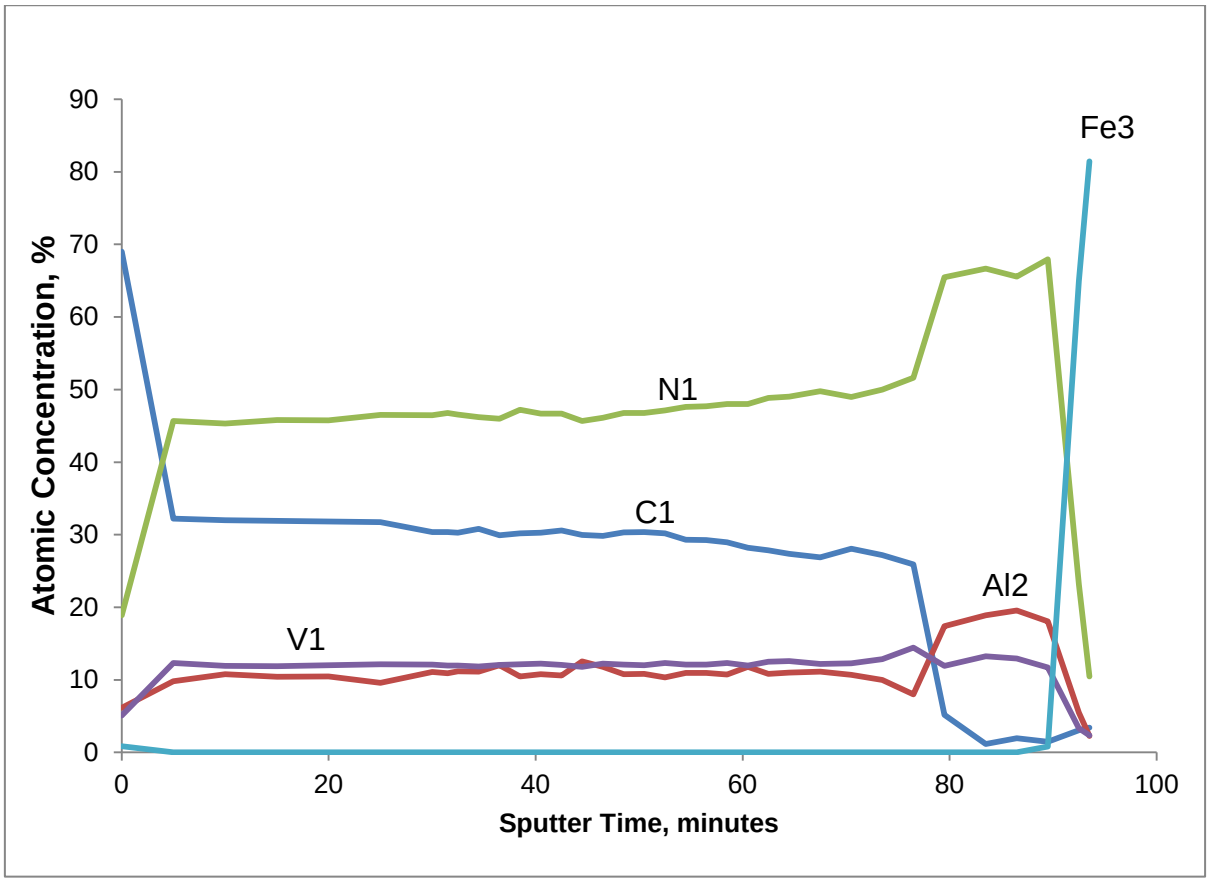
Atomic Concentration, %
Sputter Time, minutes
0
10
20
30
40
50
60
70
80
90
0
20
40
60
80
100
Fe3
N1
C1
Al2
V1

Figure 8

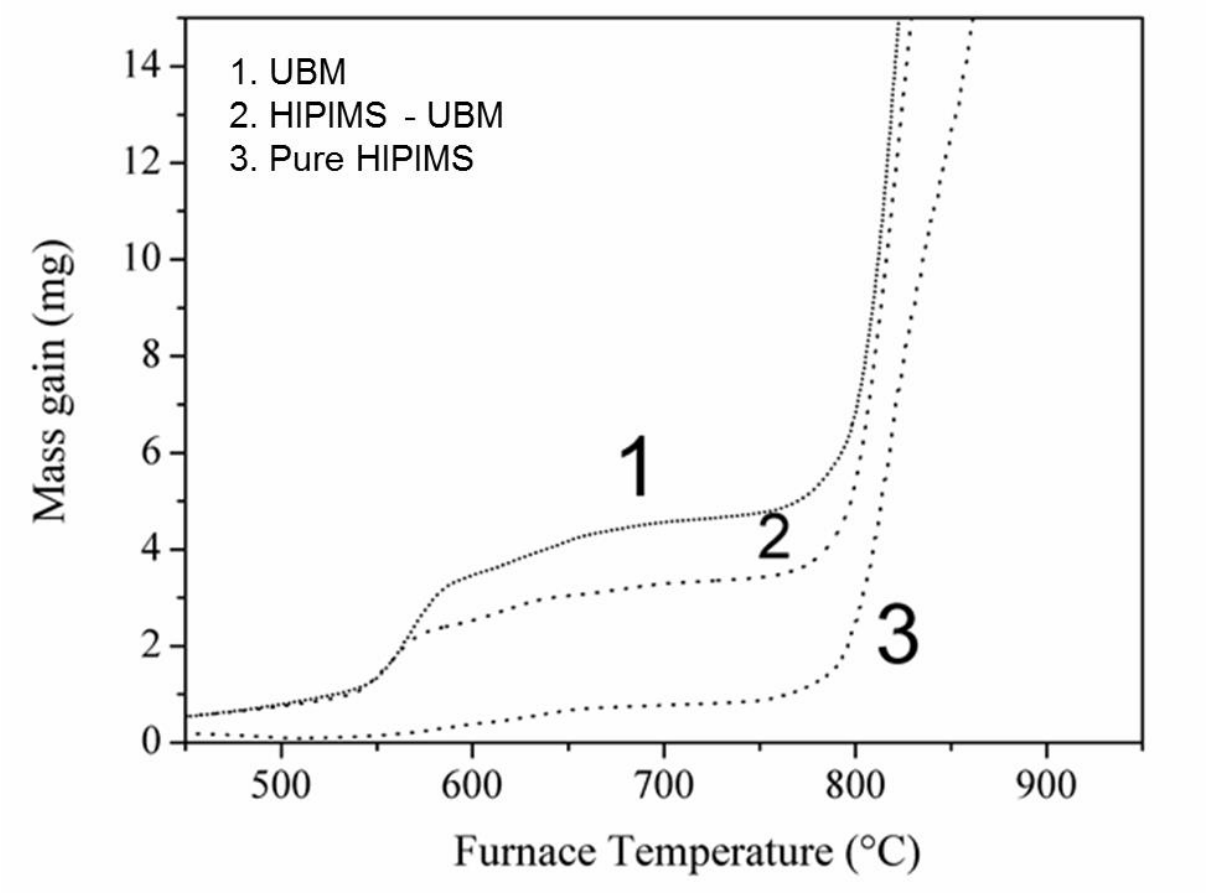
1. UBM
2. HIPIMS - UBM
3. Pure HIPIMS
Mass gain (mg)
Furnace Temperature (°C)
0
2
4
6
8
10
12
14
500
600
700
800
900
1
2
3

Figure 9

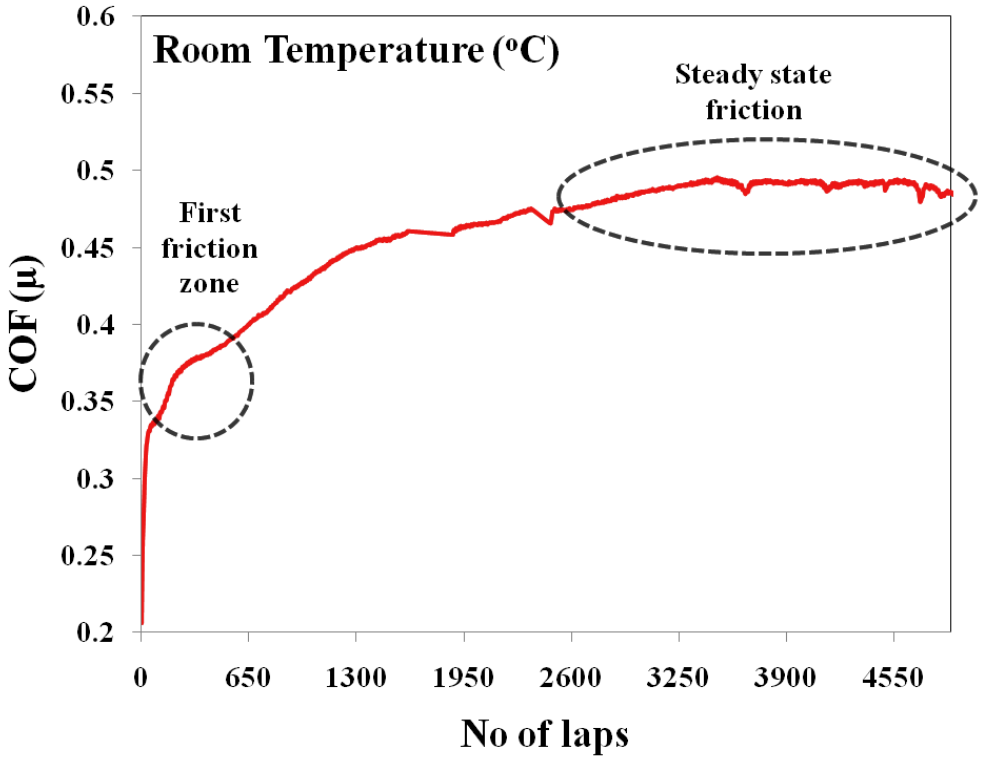

Fig 10a

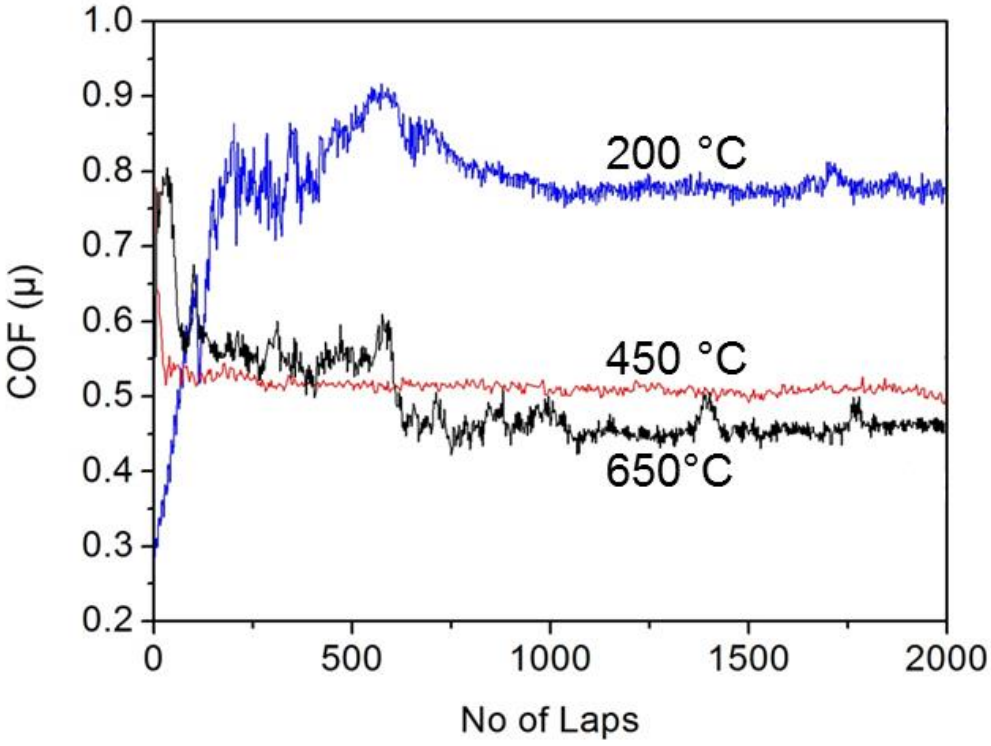

Fig. 10b

Figure 10.

Figure 11a

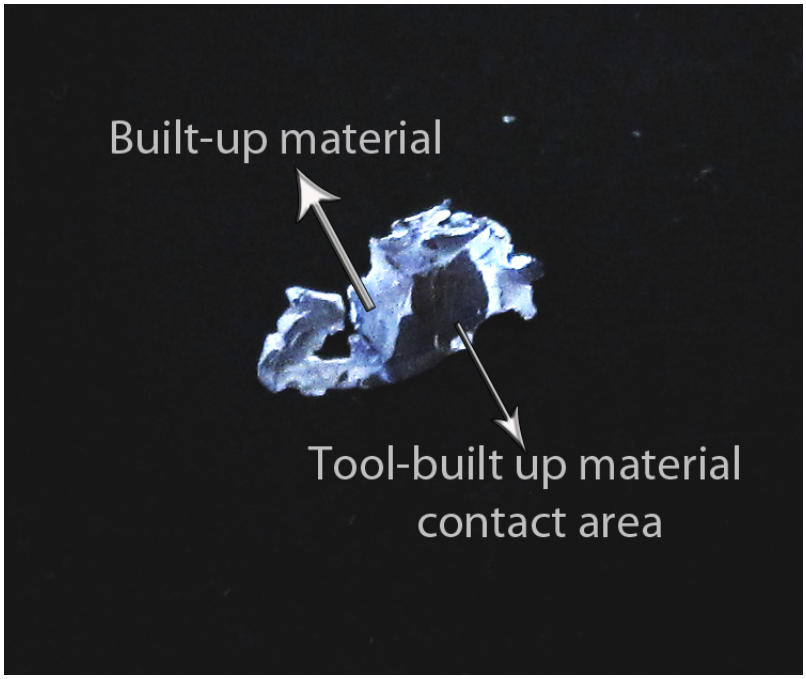

Figure 11b

Figure 11

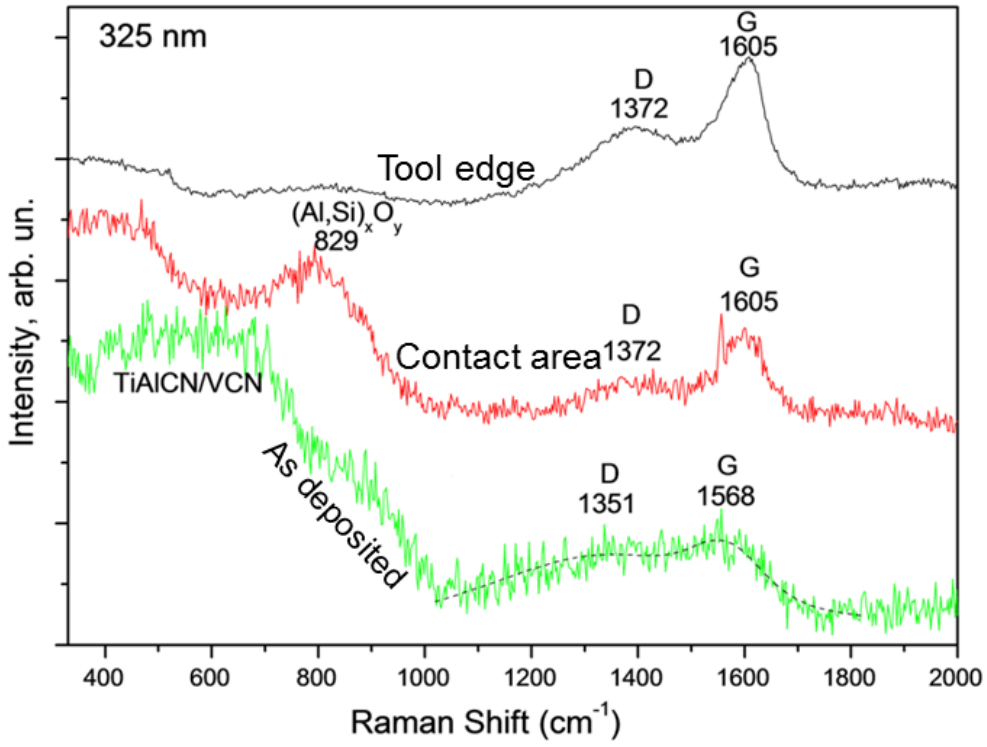

Figure 12a

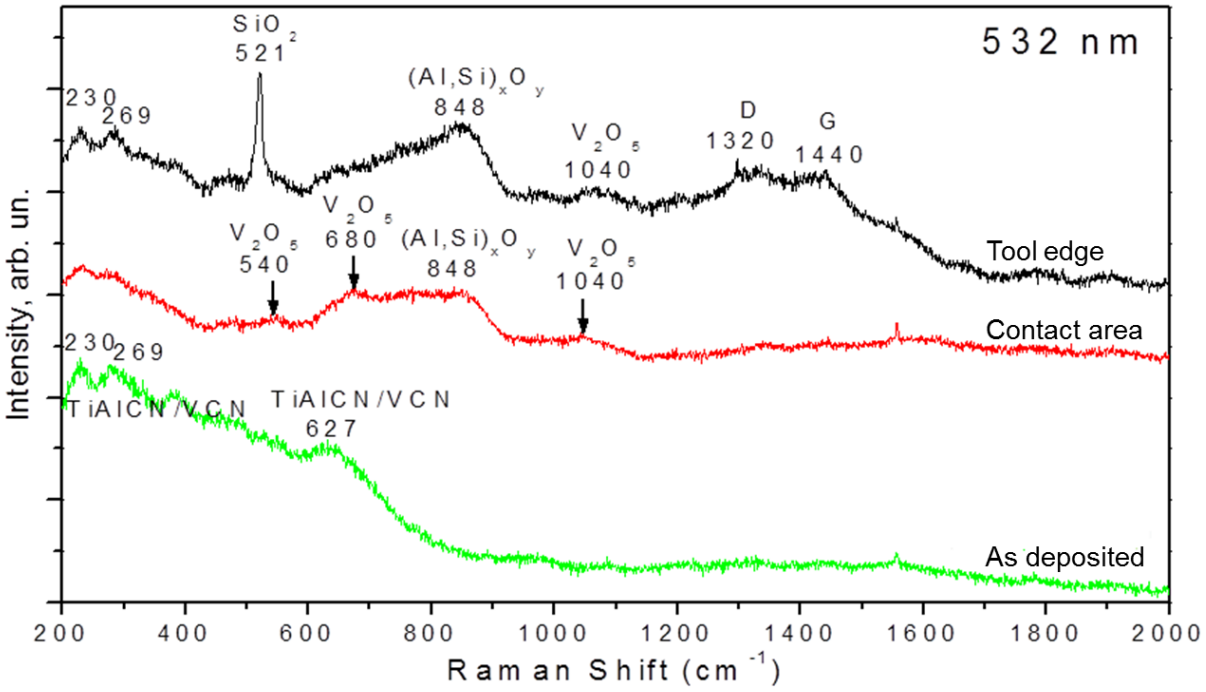

Figure 12b

Figure 12